Ergodic Outage and Capacity of Terahertz Systems Under Micromobility and Blockage Impairments

Dmitri Moltchanov, Yuliya Gaidamaka, Darya Ostrikova, Vitalii Beschastnyi, Yevgeni Koucheryavy, *Senior Member, IEEE*, and Konstantin Samouylov

***Abstract*—Terahertz (THz) communications systems are expected to become a major enabling technology at the air interface in sixth generation (6G) cellular systems. However, utilizing extremely narrow antenna radiation patterns at both base station (BS) and user equipment (UE) sides, these systems are affected by not only dynamic blockage but micromobility of UEs. To alleviate the impact of both factors one may utilize the multiconnectivity mechanism allowing for UE to remain connected to several BSs simultaneously and switch between them in case the active connection is lost. In this work, we develop a mathematical framework to characterize the outage probability and spectral efficiency associated with different degrees of multiconnectivity in dynamic blockage and micromobility environment for different beamsearching design options. Our results demonstrate that the presence of UE micromobility may have a positive impact on system performance. Particularly, multiconnectivity allows improving outage and spectral efficiency for small and medium blockers density (up to 0.5 bl./m^2) up to that of an ideal system with zero beamsearching times. Furthermore, higher gains are observed for higher degrees of multiconnectivity (e.g., greater than two) as compared to the system with only blockage impairments. For higher blockers densities, however, the reverse effect is observed.**

***Index Terms*—Terahertz communications, micromobility, spectral efficiency, outage, multiconnectivity, dynamic blockage, beamsteering.**

I. Introduction

Future 6G systems are expected to enable principally new applications at the air interface such as holographic communications, augmented/virtual reality and tactile communications [1], [2]. To satisfy the requirements of these applications 6G needs to drastically enhance the access rates of cellular technologies [3]. The terahertz band (THz, 300 GHz–3 THz) having tens of GHz of available bandwidth is nowadays considered as the major enabler for 6G air interface [4].

In addition to extraordinary promises, THz systems bring a set of principally new challenges to the system designers. THz channel properties and link-layer mechanisms have been relatively well studied so far. Particularly, the use of this band leads to extreme path losses that are principally higher even compared to millimeter wave (mmWave) band [5]. On top of this, atmospheric attenuation by the water vapor [6] adds to these losses at specific frequencies forcing the received power to fade exponentially fast [7]. Finally, similarly to mmWave systems, THz links are affected by dynamic blockage [8]. These properties have been accounted for in designs of various advanced data-link layer techniques improving the performance of THz links see, e.g., [9]–[11].

To alleviate the severe propagation losses the sub-millimeter wavelength of THz frequencies promises ultra-large antenna arrays featuring thousands of elements at both transmitter and receiver sides. These arrays will be capable of creating extremely directional steerable antenna radiation patterns with a beamwidth of just a few degrees or even less. While this property has been shown to have a positive impact on the level of interference even in extremely dense deployments [7], [12], it may also lead to much more frequent losses of connectivity. Compared to the mmWave band, where the major source of link drops is due to blockage [13], [14], in THz systems micromobility of user equipment (UE), i.e., small UE rotations and displacements in hands of a user, will also significantly contribute to connection losses.

The impact of micromobility on link-layer characteristics has been studied in [15], [16]. Particularly, in [16], the authors utilized empirical measurements and link-level simulations to reveal that the optimal antenna array size leading to the highest, on average, link capacity heavily depends on the micromobility pattern of UE. Further, in [15] they developed a mathematical framework and determined the optimal number of antenna elements to be utilized at THz base stations (BS) and UE sides to simultaneously minimize the fraction of outage time and maximize the spectral efficiency of a THz link under different types of beamsearching strategies. These studies revealed that the use of very narrow THz radiation patterns in mobile communications challenges the accuracy and speed of the employed beamsteering procedures to follow the nodes' micromobility. However, to the best of the authors' knowledge, the joint impact of micromobility and the dynamic blockage has not been studied at the system level yet.

In this study, we address the abovementioned void by analyzing fundamental UE-centric characteristics – fraction of outage time and ergodic spectral efficiency in dense THz BS deployments under micromobility and dynamic blockage. We consider 3GPP standardized multiconnectivity operation when UE simultaneously supports links to multiple THz BSs [17]. In our framework, we explicitly capture THz specific propagation characteristics and directional antenna radiation patterns as well as different designs of the beamsearching mechanisms. Finally, we characterize the gains of supporting a certain number of links for these strategies and provide a

Yu. Gaidamaka, D. Ostrikova, V. Beschastnyi and K. Samouylov are with Peoples' Friendship University of Russia (RUDN University), Moscow, Russia. Email: {gaydamaka-yuv, ostrikova-dyu, beschastnyy-va, samuylov-ke}@rudn.ru

D. Moltchanov and Y. Koucheryavy are with Tampere University, Tampere, Finland. Email: {dmitri.moltchanov, evgeni.kucheryavy}@tuni.fi

Yu. Gaidamaka and K. Samouylov are also with Federal Research Center "Computer Science and Control" of Russian Academy of Sciences, Russia.

The research was funded by the Russian Science Foundation, project no. 21-79-10139.

comparison between them.

From the technical perspective, in this study, for the first time, the joint effect of micromobility and blockage on system-level characteristics of UEs in dense THz deployments with multiconnectivity support is investigated. From the modeling viewpoint, we offer a mathematical framework that is capable of jointly capturing the effects of blockage, micromobility and multiconnectivity in a single analytically tractable model. The offered framework is capable of evaluating practical beamsearching design approaches including on-demand and periodic ones with any type of underlying search algorithm. Thus, the main contributions of our study are as follows:

- a unified mathematical framework based on probability theory and Markov chain theory for assessing the fraction of time in outage and spectral efficiency in THz BS deployments with multiconnectivity operation under dynamic micromobility and blockage impairments;
- numerical results showing that the impact of micromobility on the fraction of time in outage and spectral efficiency heavily depends on the density of blockers and the latter metric may even approach spectral efficiency of the ideal system with zero beamsearching time;
- numerical results showing that the multiconnectivity has a more profound positive impact on considered metrics as compared to the system with blockage impairments only.

The rest of the paper is organized as follows. We review the current state-of-the-art in Section II. Our system model is introduced in Section III. The performance evaluation framework is presented in Section IV. In Section V we elaborate our numerical results. Conclusions are drawn in the last section.

II. Related Work

The initial research phase related to THz communications dates back to the beginning of the last decade and was mainly focused on various aspects of physical and data link layers functionalities as well as on propagation models, see, e.g. [5], [9], [18], [19]. Over the last few years, THz communications have attracted enormous attention as one of the potential enablers for 6G radio interface [20]–[23].

Besides the added complexity caused by properties of THz-band such as significantly higher propagation losses [5], atmospheric absorption [5], [9], and blockages by dynamic and static objects [8], THz communications pose new challenges for system designers. One of these challenges is micromobility manifesting itself in small-scale shakes and rotations of UE [15], [16], [24], or antennas motion of THz BS due to environmental effects such as wind, small earthquakes, traffic, etc [24]. These fast displacements may cause frequent misalignments of the highly-directional THz beams, consequently leading to degradation of the link capacity and even outages. Particularly, the authors in [24] developed an analytical framework for characterizing expected values for the transmit and receive antenna gains in fronthaul and backhaul links under stochastic beam misalignment created by antenna movement coming from the building or antenna mast swaying. Further, the authors in [15], [16] investigate the effects of micromobility on cellular system performance. In [16], the trade-off between the antenna array size and the capacity of the THz link is studied by a combination of field measurements and link-level simulations. Employing computer simulations, the authors in [25] evaluated the optimal system and mobility parameters required for optimal throughput for mobile THz UEs. Further, in [15], the authors proposed a mathematical framework to estimate the performance of THz communications in the presence of both Cartesian and angular micromobility of the UE. Particularly, they estimated the optimal beamwidth as a function of micromobility parameters.

In contrast to traditional wireless networks, THz systems would allow for a substantially reduced size of transmitting devices. However, the smaller size of antenna elements entails reducing effective antenna aperture, which decreases the communication range. To target this effect in THz band, antenna systems with the massive number of elements are expected to be used allowing to form a directional diagram with narrow beamwidth of a few degrees [26], [27]. This extremely high directivity positively affects interference from nearby transmitters. Over the last few years, system-level studies addressing the performance of THz networks in presence of LoS blockage by moving obstacles have emerged [7], [28]–[30].

The authors in [28] modeled the multi-user interference and validated it experimentally for short-range THz communications. In [29], an analytical model for interference and signal-to-noise plus interference ratio (SINR) assessment in dense THz networks has been developed. In [7], the authors studied interference in mmWave and THz communication systems with directional antennas and blocking obstacles. In their work, the authors utilized the Taylor expansion of SINR function and calculated approximations for mean and variance of SINR. The analytical framework to investigate the interference and coverage probability for indoor THz communications with beamforming antennas is presented in [30]. In this work, the authors proposed models of line-of-sight (LoS) and non-LoS (nLoS) interference from UEs and BSs with directional beamforming antennas. Further, in [31], [32], the authors developed an analytical framework using the tools of stochastic geometry to evaluate the coverage probability of THz communication systems in a three-dimensional (3D) environment. Besides this, the study in [32] proposed an analytical framework to analyze the performance achieved by multiconnectivity strategies which are used to combat the LoS blockage effects in THz communication systems. However, the authors do not take into account practical beamsearching strategies and the micromobility phenomenon, which may also lead to additional overheads caused by beamsearching.

The study in [33] consider a multi-layer network, where there is a microwave technology (e.g., LTE) and THz one. They first characterized the exact Laplace Transform (LT) of the aggregate interference and coverage probability of a user in a THz-only network. Then, for a coexisting LTE/THz network, they derived the coverage probability of a typical user considering biased received signal power association. This is different from our study, where we consider intra-RAT multiconnectivity within THz network for an active UE, that is already associated with the network and switches between THz BSs in attempt to improve spectral efficiency and outage

metrics. On top, we consider the joint effect of micromobility and blockage with different beamsearching schemes, antenna switching times and different beamsearching designs. In [34], the authors developed a tractable analytical framework that allowed for studying coverage probability in 3D environment. The developed framework considers the effect of 3D directional antennas at both BS and UE sides, and the joint impact of the blockage caused by the user itself, moving humans, and wall blockers. The conclusion about predominant positive impact of high antenna directivity at BSs rather at the UEs delivered by the study shows agreement with our results presented in Section V.

Summarizing, the impact of micromobility is characterized at the link layer only [15], [16]. Furthermore, the authors are unaware of system-level studies evaluating the THz network performance in presence of micromobility.

III. System Model

In this section, we introduce our system model by specifying its components including propagation and antenna models, multiconnectivity operation, beamsearching algorithms as well as potential beamsearching design options. We conclude this section by introducing the metrics of interest.

A. Deployment Model

The system model is shown in Fig. 1a. We assume that the locations of THz BSs follow a Poisson point process (PPP) in $\Re^2$ with the density of λ_A. The BS height is set to h_A. We consider a single UE dropped randomly in $\Re^2$. The target UE is assumed to remain stationary. The UE height is h_U.

The humans in the pedestrian area around the UE act as potential blockers. Their spatial density in $\Re^2$ is λ_B. These blockers are modeled as cylinders and have the base radius r_B. The height of the humans is assumed constant and set to h_B, $h_B > h_U$. To capture the THz LoS blockage dynamics, we assume that humans move according to the random direction model (RDM) [35]. According to it, a user first chooses a direction of movement randomly and uniformly in $(0, 2\pi)$ and then moves in the chosen direction at constant speed v for exponentially distributed time with parameter μ.

B. Propagation and Blockage Models

As the effect of human blockage is known to be more impactful in the THz band [36]–[38], similarly to other studies, e.g., [32], we assume that no communications are feasible in LoS blockage state. The value of SINR at the UE in LoS non-blocked state can be written as [9]

$$S(x) = P_T G_{T,A} G_{T,U} \Big[\frac{x^{-\zeta_T}}{(N_0 + M_T) L_A(f,x)} \Big], \tag{1}$$

where ζ_T is path loss exponents in LoS non-blocked state, M_T is the constant capturing the interference margin, N_0 is the density of noise, P_T is emitted power, $G_{T,A}$ and $G_{T,U}$ are the BS and UE gains, $L_A(f,x)$ is the absorption losses. By following [5], [9], the absorption loss is defined as

$$L_A(f,x) = \frac{1}{\tau(f,x)}, \tag{2}$$

TABLE I: Notations

Notation	Description
λ_A	THz BS density
λ_B	density of blockers
μ^{-1}	mean blocker passage time
r_B	blocker radius
h_B	blocker height
h_U	UE height
h_A	THz BS height
v	blocker speed
$L_A(f,r)$	absorption loss
$K(f)$	absorption coefficient
P_T	BS emitted power
$G_{T,A}$	BS antenna array gain
$G_{T,U}$	UE antenna array gain
ζ_T	path loss exponent in LoS non-blocked state
M_T	shadow fading and interference margin
p_B	blockage probability
$x(t)$, $y(t)$	random displacements processes over x and y axis
$\phi(t)$, $\theta(t)$	random rotation processes over these plane
$\mathrm{erfc}(\cdot)$	complementary error function
$\mu_{(\cdot)}$, $\sigma_{(\cdot)}$	micromobility parameters
α	array HPBW
θ_m	array maximum
$\theta^{\pm}_{3dB}$	upper and lower 3-dB points
δ	array switching time
$N_{(\cdot)}$	number of antenna array elements
$N_U \times N_U$	number of UE antenna array elements
$N_T \times N_T$	number of THz BS antenna array elements
C	mean capacity
T_A	period before beam misalignment
T_B	beamsearching duration
T_L	non-blocked state period
T_{NL}	blocked state period
T_P	periodic beam update interval
p_N	probability of simultaneous LoS blockage at all N THz BSs
p_O	outage probability
p_{T_i}	share of time being associated with is BS
N	number of THz BSs
$E[B]$	mean beamsearching time within LoS non-blocked timespan
B_i	LoS blocked period with i-s BS
$E[C_i]$	mean UE capacity when associated with i-s BS
N_0	density of noise
r	communication distance

where $\tau(f,r)$ is the transmittance of the medium following the Beer-Lambert law, $\tau(f,r) \approx e^{-K(f)x}$, $K(f)$ is the overall absorption coefficient of the medium. The frequency-dependent absorption coefficient $K(f)$ can be represented as [5]

$$K(f) = \sum_{i,g} k^{i,g}(f), \tag{3}$$

where $k^{i,g}(f)$ represents individual absorption coefficient for the isotopologue i of gas g. We utilized the air in the office environment having 78.1% of nitrogen and 20.9% of oxygen, at standard altitude, water vapor fraction of 2%. The coefficients $k^{i,g}$ are available from the HITRAN database [39]. For practical calculation of the overall absorption coefficient in the considered band, we utilize the worst-based approximation, $K = \max_f K(f)$ leading to the SNR in the following form

$$S(x) = P_T G_{T,A} G_{T,U} \Big[\frac{x^{-\zeta_T} e^{-Kx}}{N_0 + M_T} \Big]. \tag{4}$$

Finally, the absorption phenomena may also lead to the molecular noise theoretically predicted in [5]. However, recent measurements [40] did not reveal any noticeable impact of

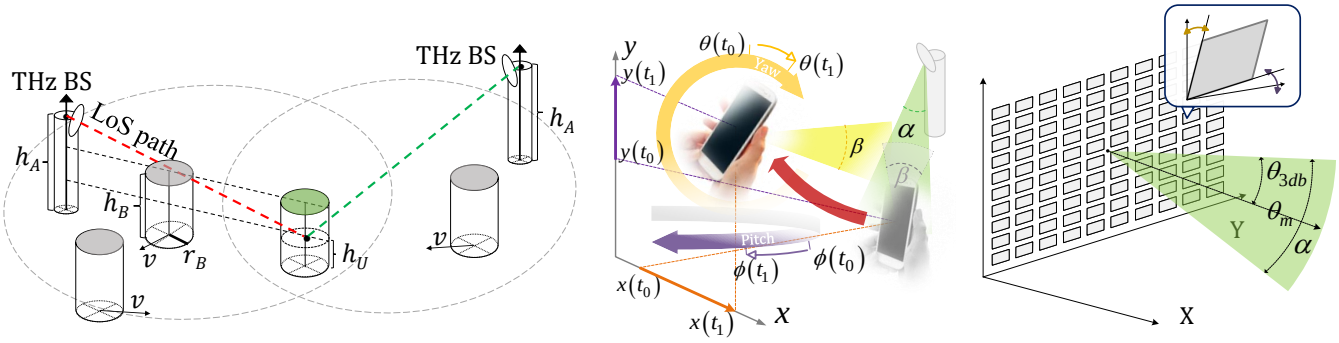

(a) Deployment (b) Micromobility (c) Antenna

Fig. 1: The elements on the considered THz communications system model.

molecular noise phenomenon. Nevertheless, if one would like to incorporate this effect into the model, the molecular noise term, N_M, has to be included in the denominator of (4). By following [7], [9] N_M can be approximated by $S'(x)[1-\tau(f,x)]$, where where $\tau(f,x)$ is the transmittance of the medium, $S'(x)$ is the power at the distance x without the thermal noise.

Observe, that in our study we capture interference by a constant – so-called interference margin. The rationale is that following recent studies of THz communications systems [7], [41], utilizing extremely directional antenna radiation patterns at BSs the impact of interference is expected to be negligible. If one wants to explicitly include the effect of interference it can be done by, e.g., applying the Campbell theorem as shown in [12], [42] or by utilizing LT to get probability density function (pdf) of interference according to [43] for the further use in the framework proposed in our paper. This will not drastically affect our methodology.

C. Micromobility Model

The micro-mobility refers to small shakes and rotations of UE in hands of a user when he/she perceives a certain service. These impairments may affect communications even when a user is stationary. Observe that the system enters the outage state when the center of the UE beam leaves the circularly shaped area corresponding to half-power beamwidth (HPBW) of THz BS. It could happen due to small displacements of UE over Ox- and Oy-axes as well as due to yaw (vertical axis) and pitch (transverse axis) motions of UE in the user's hands. Observe that small displacements over Oz-axis as well as roll (longitudinal axis) motion do not severely affect the communications. The rationale is that these small-scale displacements are limited to just a few tens of centimeters while the roll does not change antenna alignment.

To represent the micromobility process at UE we utilize the model introduced in [15]. According to it, the micromobility is modeled as a combination of random displacement processes over Cartesian $y(t)$ and $x(t)$ axes, together with the random rotation processes in these planes, $\phi(t)$ and $\theta(t)$, see Fig. 1b. Assuming the Brownian motion nature of these movements the authors in [15] revealed that the pdf of time to outage due to beam misalignment $f_{T_A}(t)$ follows (5), where $\mathrm{erfc}(\cdot)$ is the complementary error function, $\mu_{(\cdot)}$ and $\sigma_{(\cdot)}$ are the parameters of the corresponding displacement and rotation components that can be estimated from the empirical data as shown in [15]. Note that instead of the Brownian motion model proposed in [15] more comprehensive UE micromobility models can be utilized, e.g. Markov models, as long as they allow for explicit characterization of FPT time.

D. Antenna Models and Beamsearching Algorithms

We assume planar antenna arrays at both the BS and the UE. Similarly to [44], [45], we utilize a cone model with the beamwidths corresponding to HPBW of the antenna radiation pattern illustrated in Fig. 1c. Using [46] the mean antenna gain over HPBW is given by

$$G = \frac{1}{\theta^{+}_{3db} - \theta^{-}_{3db}} \int_{\theta^{-}_{3db}}^{\theta^{+}_{3db}} \frac{\sin(N_{(\cdot)}\pi\cos(\theta)/2)}{\sin(\pi\cos(\theta)/2)} d\theta, \qquad (6)$$

where $N_{(\cdot)}$ is the number of antenna elements in the appropriate plane. The HPBW of the array, α, can be determined as $\alpha = 2|\theta_m - \theta^{\pm}_{3db}|$, where θ_m is the array maximum that can be computed as $\theta_m = \arccos(-1/\pi)$, $\theta^{\pm}_{3db}$ are the upper and lower 3dB points estimated as $\theta^{\pm}_{3db} = \arccos[\pm 2.782/(N_{(\cdot)}\pi)]$.

The antenna is 3D one with conical representation of the main lobe similar to the one utilized in [12], [42] when studying interference in 3D mmWave deployments. However, contrarily to [7], where the antenna gain has been obtained as a function of HPBW angle, here, we utilize the results of [46] providing both HPBW angles and associated gains as a function of antenna elements in the appropriate plane. For each plane, we utilize (6) to determine these parameters. For practical calculations we employ HPBW approximation given by $102^\circ/N$. [46], [47]. Similarly, the linear gain can be approximated by the number of elements [46].

In the considered scenario the decision on how to efficiently utilize THz BSs heavily depends on the interplay between beamsearching time and time to outage caused by micromobility. Thus, we consider two beamsearching procedures:

- *Exhaustive search.* In this case, all the available antenna configurations at both the BS and the UE are successively attempted. The beamsearching time of this approach is $T_B = N_U N_T \delta$, where N_U and N_T are the numbers of UE and THz BS antenna array configurations and δ is the array switching time.

$$f_{T_A}(t)=\frac{\frac{e^{-\frac{(\log(t)-\mu_x)^2}{2\sigma_x^2}}}{\sigma_x}\left[2-\mathrm{erfc}\left(\frac{\mu_y-\log(t)}{\sqrt{2}\sigma_y}\right)\right]+\frac{e^{-\frac{(\log(t)-\mu_y)^2}{2\sigma_y^2}}}{\sigma_y}\left[2-\mathrm{erfc}\left(\frac{\mu_x-\log(t)}{\sqrt{2}\sigma_x}\right)\right]}{4\sqrt{2\pi}t\left[1-\frac{1}{2}\mathrm{erfc}\left(\frac{\mu_\phi-\log(t)}{\sqrt{2}\sigma_\phi}\right)+\frac{1}{2}\mathrm{erfc}\left(\frac{\mu_\theta-\log(t)}{\sqrt{2}\sigma_\theta}\right)\right]^{-1}}+\frac{\frac{e^{-\frac{(\log(t)-\mu_\phi)^2}{2\sigma_\phi^2}}}{\sigma_\phi}\left[2-\mathrm{erfc}\left(\frac{\mu_\theta-\log(t)}{\sqrt{2}\sigma_\theta}\right)\right]+\frac{e^{-\frac{(\log(t)-\mu_\theta)^2}{2\sigma_\theta^2}}}{\sigma_\theta}\left[2-\mathrm{erfc}\left(\frac{\mu_\phi-\log(t)}{\sqrt{2}\sigma_\phi}\right)\right]}{4\sqrt{2\pi}t\left[1-\frac{1}{2}\mathrm{erfc}\left(\frac{\mu_x-\log(t)}{\sqrt{2}\sigma_x}\right)+\frac{1}{2}\mathrm{erfc}\left(\frac{\mu_y-\log(t)}{\sqrt{2}\sigma_y}\right)\right]^{-1}} \quad (5)$$

- *Iterative search.* As an alternative approach, we consider an iterative beamsearching algorithm realized with sector level sweep and beam refinement procedures, as utilized in, e.g., IEEE 802.11ad/ay [48]. The beamsearching time of this scheme is $T_B=(N_U+N_T)\delta$.

E. Connectivity Schemes and System Design Options

To evaluate the effect of multiconnectivity on UE performance, we assume that the tagged UE can maintain N, $N=1,2,\ldots$ links to neighboring THz BSs. The choice of BSs is based on the time-averaged SINR metric [49]. Since the latter is a monotonously decreasing function of the distance, N nearest BSs are selected by the UE at the session initiation time. However, at a given time instant UE utilizes only a single link with the highest SINR for communications.

In presence of micromobility, the outage might happen much more frequently compared to mmWave systems that are mainly affected by the blockage. Thus, in addition to different types of beamsearching procedures, we consider the following connectivity design schemes:

- *Ideal design*. In this case, we assume that no overhead is induced by the beamsearching procedure. In other words, the change of the active BS is performed instantaneously with no delay caused by the search procedure. This scheme is utilized to serve as an upper bound for the rest of the design options.
- *Periodic design*. In this case, the instant of time when the beamalignment procedure is invoked is determined by two events, expiration of the beam update timer, T_P, or outage event, whichever happens first.
- *On-demand design*. In this case, the beamalignment procedure is invoked only when outage is experienced. Correspondingly, the THz BS, UE is associated with, is changed every time the UE experiences an outage as a result of blockage or micromobility.

F. Metric of Interest

We concentrate on two fundamental metrics for cellular THz deployments – ergodic outage probability and ergodic spectral efficiency. Here, the term ergodic means time-averaging, implying that the former metric coincides with the fraction of time UE does not have network connectivity and can be referred to as "non-connection" or "non-communication" probability. Ergodic spectral efficiency also implies averaging over time characterizing time-averaged spectral efficiency. From now on, we refer to these metrics as outage and spectral efficiency silently assuming the abovementioned definitions.

IV. Performance Evaluation Framework

In this section, we develop our performance evaluation framework. We successively consider the ideal, on-demand, and periodic design schemes and capture the details of the considered multiconnectivity and beamsearching operations.

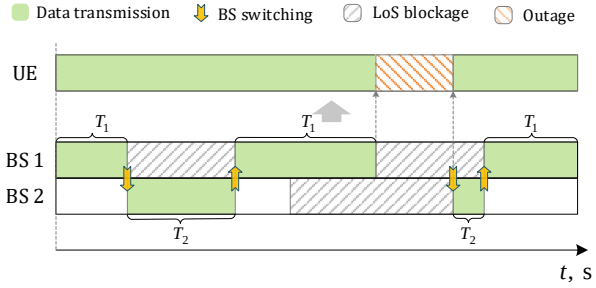

Fig. 2: Time diagram of the ideal design scheme.

A. Ideal Beamsearching

Consider first the scheme, where the beamsearching procedure is instantaneous. In this scheme, the UE first selects its nearest BS. The UE changes its association point whenever it enters the outage state with the current BS. The outage can be caused by micromobility or by blockage of the LoS path by human bodies. At both session initiation and re-association time instants, the closest non-blocked BS out of the nearest N is chosen. The scheme with instantaneous beamalignment is illustrated in Fig. 2, where the UE is associated with the two closest BSs and experiences outage conditions only when both of them are in blocked conditions.

The pdf of distance to i-s neighbor in the Poisson field of THz BSs is available from [50]

$$f_i(x)=\frac{2(\pi\lambda_A)^i}{(i-1)!}x^{2i-1}e^{-\pi\lambda_A x^2},\ x>0,\ i=1,\ldots,N. \quad (7)$$

Thus, the UE capacity when associated with i-s BS is

$$E[C_i]=\int_0^\infty \log_2(1+S(x))\,f_i(x)\,dx. \quad (8)$$

while the blockage probability to i-s THz BS is given by

$$p_{N,i}=1-\int_0^\infty \frac{2(\pi\lambda_A)^i}{(i-1)!}x^{2i-1}e^{-\pi\lambda_A x^2}e^{-2xr_B\lambda_B\frac{h_B-h_U}{h_A-h_U}}dx. \quad (9)$$

Assuming that the LoS blockage processes at THz BSs are independent of each other, the probability p_N that all N selected BSs are simultaneously blocked can be written as

$$p_N=\prod_{i=1}^{N}p_{N,i}, \quad (10)$$

and coincides with the outage probability, i.e., the fraction of time when data transmission is impossible, $p_O=p_N$.

The fraction of time UE is associated with i-s BS is then

$$p_{T_i}=(1-p_{N,i})\prod_{k=1}^{i-1}p_{N,k}. \quad (11)$$

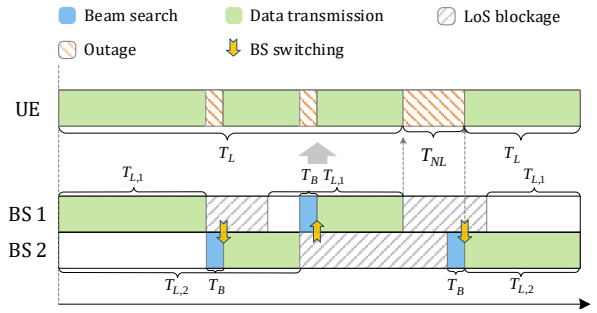

Fig. 3: On-demand design scheme without micromobility.

leading to the following spectral efficiency

$$E[C] = \sum_{i=1}^{N} p_{T_i} E[C_i]. \tag{12}$$

B. On-Demand Beamsearching Without Micromobility

We now proceed considering the on-demand scheme reflecting WLAN design style of THz communications system. We start with the system, where outage events may only be caused by blockage. From the practical perspective, the beamalignment is invoked when an outage happens while, technically, we now need to extend the ideal beamsearching approach by taking into account non-zero time to switch to another BS by introducing an additional component, T_B. Note that in practice, T_B depends on many factors, including the employed beamsearching algorithms, the size of the antenna arrays, and the time it takes to assess a single beam configuration.

When the UE may only associate with its nearest N BSs, the connectivity pattern comprises two periods, connectivity interval T_L and outage interval T_{NL}. Note that T_{NL} is interpreted as the time duration when there are no BSs in non-blocked state. In its turn, T_L starts when the UE associates with its closest non-blocked BS for the first time after T_{NL} and ends when there are no BSs in non-blocked state. Note that since $T_L \gg T_B$, we also assume that the beamsearching procedure cannot be interrupted by LoS blockage.

The time diagram in Fig. 3 illustrates the considered scheme for the case of $N = 2$ BSs outlining the possible events and states defined by the model. LoS blockage triggers outage periods that end with a beamsearching procedure. Thus, an outage period consists of the period when all N BSs are in blocked state, T_{NL}, and the time needed for beamsearching, T_B. Alternatively, it may comprise of just beamsearching procedure in case there is at least one BS in non-blocked state. BS switching occurs only as a result of beamsearching procedure that establishes a new active connection with the nearest BS in the LoS non-blocked state.

Following [47], [51] the time between successive blockage events under RDM mobility pattern is approximately exponentially distributed. Thus, the process of blockage events with i-s BS is homogeneous Poisson with the mean intensity of $\mu_{B,i}$ provided by [51]

$$\mu_{B,i} = \int_0^{\infty} f_i(x) \frac{2r_B \lambda_B v (x[h_B - h_U] + r_B[h_A - h_U])}{(h_A - h_U)} dx, \tag{13}$$

implying that pdf and cumulative distribution function (CDF) of LoS non-blocked period when associated with i-s BS are provided by $f_{T_{L,i}}(t) = \mu_{B,i} e^{-\mu_{B,i} t}$ and $F_{T_{L,i}}(t) = 1 - e^{-\mu_{B,i} t}$.

Let $F_{B,i}(t)$ be CDF of the blocked period with i-s BS. As demonstrated in [52] the distribution of the blocked interval coincides with the busy period in $M/GI/\inf$ system

$$F_{B,i}(t) = 1 - \left(\int_0^t [1 - F_{B,i}(t-z)] \left| de^{-\mu_{B,i} F_T(z)} \right| + \right. \tag{14}$$
$$\left. + [1 - F_T(t)] \left[1 - \int_0^t [1 - F_{B,i}(t-z)] e^{-\mu_{B,i} F_T(z)} \mu_{B,i} dz \right] \right),$$

where $F_T(t)$ is the CDF of time required for a single blocker to cross the LoS blockage zone. Since the length of the LoS blockage zone associated with UE is much greater than its width [53], it is safe to assume that the blockers enter the blockage zone at the right angle to the long side. Thus, they spend $2r_B/v$ amount of time to cross it. In this case, F_T has the form of the Heaviside step function $F_T(t) = H(t - 2r_B/v)$.

Assuming independence of blockage processes at the BSs, the CDF of the blocked period, $T_{NL,i}$, conditioned on the event that the index of the previous BS, UE was associated with, is i, is delivered by

$$F_{T_{NL,i}}(t) = 1 - [1 - F_{B,i}(t)] \prod_{j=1, j\neq i}^{N} \left[1 - F_{B_j^*}(t) \right], \tag{15}$$

where B_i and B_j^* are the random variables (RVs) denoting blockage and residual blockage periods when associated with i-s and j-s BSs, respectively, while $F_{B,i}(x)$ and $F_{B^*,j}(x)$ are the corresponding CDFs. The latter unknown term is provided by

$$F_{B^*,j}(t) = \int_0^{\infty} \frac{F_{B,i}(t+\tau) - F_{B,i}(\tau)}{\tau[1 - F_{B,i}(\tau)]} d\tau, j = 1, \ldots, N, j \neq i. \tag{16}$$

Finally, we arrive at the mean length of the LoS blocked period followed by beamsearching in the following form

$$E[T_{NL}] = T_B + \sum_{i=1}^{N} p_{T_i} \int_0^{\infty} t f_{T_{NL,i}}(t) dt, \tag{17}$$

where p_{T_i} is obtained in (11), $f_{T_{NL,i}}(t)$ is obtained in (15).

Consider now a connectivity interval, T_L, defined as the time interval when there is always a BS in non-blocked state out of all N available BS, that UE may associate with. We are now in the position to introduce the model of the switching process between BS by utilizing an absorbing Markov chain demonstrated in Fig. 4, where the state number i represents i-s nearest BS, while the $j = N+1, \ldots, 2N$ states denote the beamsearching procedure after LoS blockage with j-s BS. Particularly, the states $i = 1, \ldots, N$ represent active communication periods with i-s BS, while the states $N+i$, $i = 1, \ldots, N$ correspond to beamsearching procedure caused by LoS blockage when associated with i-s BS. The absorbing state "0" designates the end of the connectivity period and the beginning of outage interval when all BS are blocked.

The states of absorbing Markov chain are divided into two non-overlapping subsets: transient and absorbing states. In

our model, we have $2N$ transient and one absorbing state. Markov chain is characterized by initial vector $\vec{\pi}$ and matrix of transition probabilities $Q=[q_{ij}]$, $i,j=0,...,2N$. Since we assume that session is always initiated in the non-blocked state, the initial vector for the considered chain is $\vec{\pi}$, where $\pi_i = p_{T_i}(1-p_N)^{-1}$, when $i=1,\ldots,N$, and $\pi_i=0$, when $i=0,N+1,\ldots,2N$. Finally, transition probability matrix Q is a square reducible matrix, and, whereas the states of the chain are non-recurrent, the diagonal elements of the matrix are all zeros. Recall that the probability of jumping from i to j in exactly k steps is the (i,j)-entry of Q^k.

Observe that the period when UE is associated with i-s BS can only be interrupted by LoS blockage event. Thus, the probability of entering the state $N+i$ when associated with i-s BS equals to $1-\prod_{k=1}^{N} p_{N,k}$, i.e., $q_{i,N+i}=\prod_{k=1}^{N} p_{N,k}$, $i=1,\ldots,N$, while the probability of simultaneous blockage at all N BSs was found in (10). The need for having N states $j=N+1,...,2N$, representing beamsearching procedure after LoS blockage stems from the fact that once UE enters the LoS blocked conditions with the i-s BS, it cannot resume association with this BS after beamsearching unless the blockage finishes within the beamsearching duration. This is in contrast with beamsearching after beam misalignment as in the latter case the choice of BS does not depend on the BS, UE was previously associated with, see Subsection IV-C. Therefore, the probability of associating with i-s BS after LoS blockage at the same BS is conditioned on blockage duration leading to the following probability

$$q_{N+i,i} = F_{T_{NL,i}}(T_B)(1-p_{N,i})\prod_{k=1,k\neq i}^{i-1} p_{N,k}, i=1,\ldots,N. \quad (18)$$

Summarizing the abovementioned expositions, the transition probabilities $Q=[q_{ij}]$, $i,j=0,\ldots,2N$, of the considered Markov model chain are given by

$$\begin{aligned}
&q_{i,N+i} = 1-p_N, i=1,\ldots,N,\\
&q_{N+i,i} = F_{T_{NL,i}}(T_B)(1-p_{N,i})\prod_{k=1,k\neq i}^{i-1} p_{N,k}, i=1,\ldots,N,\\
&q_{N+j,i} = (1-p_{N,i})\prod_{k=1,k\neq i}^{i-1} p_{N,k}, i,j=1,\ldots,N, i\neq j,\\
&q_{i,0} = \prod_{k=1}^{N} p_{N,k}, i=1,\ldots,N,\\
&q_{0,0} = 1,\\
&q_{i,j} = 0, \text{ otherwise.}
\end{aligned} \quad (19)$$

Recall that the mean number of times the absorbing Markov chain visits a transient state is determined by the elements of fundamental matrix $D=(I-U)^{-1}$ [54], where $U=[u_{ij}=q_{ij}]$, $i,j=1,...,2N$ is the submatrix describing the process before leaving the set of transient states. The (i,j) entry of the matrix D is the expected number of times the chain is in the state j, given that the chain started in state i. By utilizing the fundamental matrix, the mean number of steps from the state

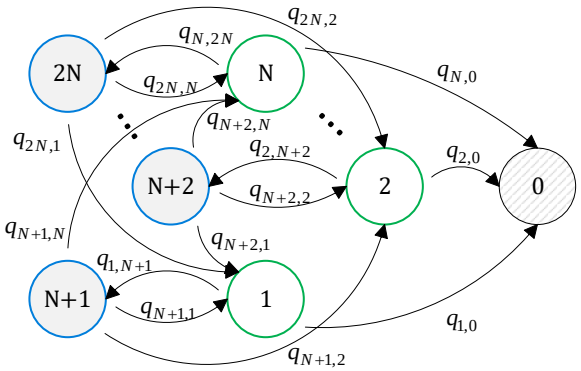

Fig. 4: Model for on-demand scheme without micromobility.

i before absorption is given by the corresponding elements of vector $\vec{\tau}$ with the following components

$$\tau_i = \sum_{j=1}^{2N} \pi_j d_{ji}, i=1,\ldots,2N. \quad (20)$$

By utilizing this result, the mean beamsearching duration in LoS non-blocked state can be written as

$$E[B] = T_B \sum_{j=N+1}^{2N} \tau_{N+j}. \quad (21)$$

leading to the mean duration of connectivity interval

$$E[T_L] = E[B] + \sum_{i=1}^{N} \tau_i T_{L,i}, \quad (22)$$

where $T_{L,i}$ is the mean duration of continuous association with i-s BS that can be found as

$$T_{L,i} = \int_0^\infty t f_{T_{L,i}}(t) dt. \quad (23)$$

The latter provides us the opportunity to define the fraction of time UE is associated with i-s BS as the ratio between the mean time in this state to the whole time before absorption. By utilizing this observation the mean spectral efficiency during T_L is provided by

$$E[C_{T_L}] = \frac{1}{E[T_L]} \sum_{i=1}^{N} \tau_i T_{L,i} E[C_i]. \quad (24)$$

Finally, writing the outage probability as

$$p_O = \frac{E[T_{NL}] + E[B]}{E[T_{NL}] + E[T_L]}, \quad (25)$$

we arrive at the spectral efficiency in the following form

$$E[C] = \frac{E[T_L]}{E[T_{NL}] + E[T_L]} E[C_{T_L}]. \quad (26)$$

Note that by construction, (25) represents "non-connection" or "non-communication" probability, while (26) evaluates spectral efficiency averaged over time.

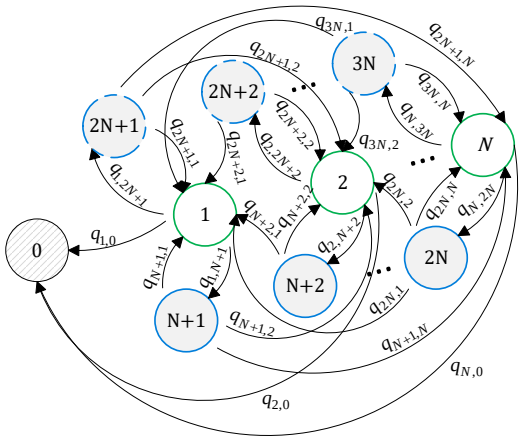

Fig. 5: Model for the on-demand design with micromobility.

C. On-Demand Beamsearching with Micromobility

We now proceed to integrate the effect of micromobility into the model. Observe that this can be done by adding "beamforming" states $2N+i$, $i=1,\ldots,N$, to the previously introduced Markov chain as shown in Fig. 5. Particularly, $i=N+1,\ldots,2N$ states correspond to beamsearching due to blockage, while $i=2N+1,\ldots,3N$ states represent beamsearching due to beam misalignment. The time diagram for the communication pattern shown in see Fig. 6 now includes beam misalignment that triggers beamsearching procedures independently from LoS blockage events. Recall that beam misalignment may only occur in LoS non-blocked conditions and its duration is characterized by (5).

The transition probabilities $q_{2N+i,i}, i=1,\ldots,N$, represent probabilities of being associated with i-s BS as the result of beamsearching procedure caused by beam misalignment. Since the probability to associate with BS in LoS non-blocked conditions does not depend on the micromobility, the transition probabilities are determined similarly to (19). However, these probabilities should be conditioned on the event that the last associated BS is still in non-blocked state, i.e.,

$$q_{2N+i,i}=\prod_{k=1}^{i-1}p_{N,k}, i=1,\ldots,N, \tag{27}$$

when the association is resumed with the current BS, and

$$q_{2N+i,j}=(1-p_{N,i})\prod_{k=1,k\neq i}^{j-1}p_{N,k}, i,j=1,\ldots,N, i\neq j, \tag{28}$$

when UE is switched to another BS in non-blocked conditions.

The time interval when UE is associated with i-s BS can be interrupted by either beam misalignment or LoS blockage event. In the case of beam misalignment, the probability of entering the state $2N+i$ when associated with i-s BS can be found as the probability of beam misalignment occurring sooner than LoS blockage at i-s BS, i.e.,

$$q_{i,2N+i}=(1-p_N)\int_0^\infty\int_y^\infty f_{T_A}(y)\,f_{T_{L,i}}(x)dxdy, i=1,\ldots,N. \tag{29}$$

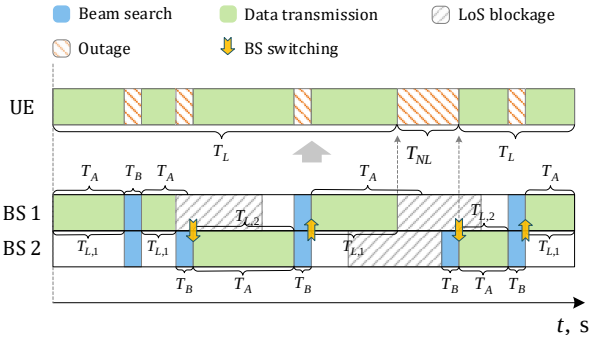

Fig. 6: On-demand design scheme with micromobility.

Similarly, the probability of entering state $N+i$ when associated with i-s BS can be found by utilizing the complementary probability, that is,

$$q_{i,N+i}=(1-p_N)\int_0^\infty\int_y^\infty f_{T_{L,i}}(y)\,f_{T_A}(x)dxdy, i=1,\ldots,N. \tag{30}$$

The elements of $Q=[q_{ij}]$, $i,j=0,...,3N$ can be written as

$$\begin{aligned}
&q_{i,N+i}=(1-p_N)\int_0^\infty\int_y^\infty f_{T_{L,i}}(y)\,f_{T_A}(x)dxdy, i=1,\ldots,N,\\
&q_{i,2N+i}=(1-p_N)\int_0^\infty\int_y^\infty f_{T_A}(y)\,f_{T_{L,i}}(x)dxdy, i=1,\ldots,N,\\
&q_{N+i,i}=\prod_{k=1}^{i-1}p_{N,k}, i=1,\ldots,N,\\
&q_{N+i,j}=(1-p_{N,j})\prod_{k=1,k\neq i}^{j-1}p_{N,k}, i,j=1,\ldots,N, i\neq j,\\
&q_{2N+i,i}=\prod_{k=1}^{i-1}p_{N,k}, i=1,\ldots,N,\\
&q_{2N+i,j}=(1-p_{N,j})\prod_{k=1,k\neq i}^{j-1}p_{N,k}, i,j=1,\ldots,N, i\neq j,\\
&q_{i,0}=p_N, i=1,\ldots,N,\\
&q_{0,0}=1,\\
&q_{i,j}=0, \text{otherwise}.
\end{aligned} \tag{31}$$

Now, the mean duration of continuous association with i-s BS can be similarly found from the minimum of two RVs as

$$T_{L,i}=\int_0^\infty t\left(f_{T_{L,i}}(t)\left[1-F_A(t)\right]+f_{T_A}(t)\left[1-F_{T_{L,i}}(t)\right]\right)dt. \tag{32}$$

The rest of the metrics for this scheme can be found similarly to the on-demand scheme without micromobility derived in Subsection IV-B by changing the upper limit in sums from "$2N$" to "$3N$" in (20)-(21).

D. Periodic Beamsearching with Micromobility

Finally, we consider the periodic design scheme. The principle difference of this scheme from the on-demand one addressed in Subsection IV-C is that the active communication can be interrupted not only by beam misalignment and LoS

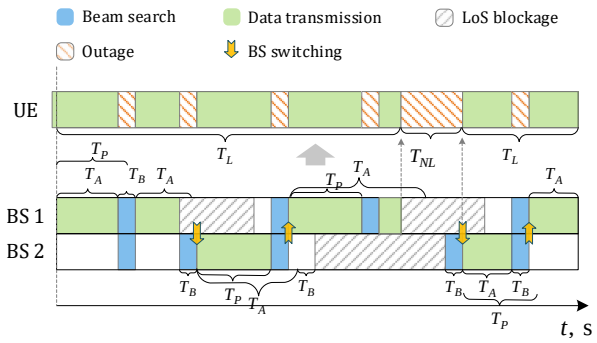

Fig. 7: Periodic design scheme with micromobility.

blockage but also by periodic beamalignment that is launched every T_P s. One may immediately observe that in this case the CDF of the time to next periodic alignment procedure can be described by a step function $F_{T_P}(t) = H(t - T_P)$.

Since the choice of the next BS does not depend on the current BS, the beamalignment procedure is similar to the one that is caused by beam misalignment. Thus, we can capture both procedures by utilizing the $i = 2N+1, \ldots, 3N$ states of the Markov chain as proposed in Section IV-C. Recall, that in the on-demand scheme with micromobility we defined the transition probabilities as the minimum of two RVs: (i) time to beam misalignment T_A, and (ii) time to LoS blockage when associated with i-s BS. Now, to capture the behavior of periodic beamalignment we have to complement these RVs with the time to periodic alignment T_P and consider the minimum of two RVs and constant time T_P.

Consider the probability of beamsearching due to beam misalignment or periodic alignment occurring sooner than LoS blockage at i-s BS, $p_{M,i}$. For this probability we have

$$p_{M,i} = \int_0^\infty \int_y^\infty f_{T_A}(y)\left[1 - F_{T_P}(y)\right] f_{T_{L,i}}(x) dx dy + \\ + \int_0^\infty f_{T_A}(x) F_{T_P}(x) dx \int_0^\infty f_{T_{L,i}}(x) F_{T_P}(x) dx, i, = 1, \ldots, N. \quad (33)$$

The latter implies that the elements of Q are provided by

$$\begin{aligned}
&q_{i,N+i} = (1 - p_N)(1 - p_{M,i}), i = 1, \ldots, N, \\
&q_{i,2N+i} = (1 - p_N)(p_{M,i}), i = 1, \ldots, N, \\
&q_{N+i,i} = \prod_{k=1}^{i-1} p_{N,k}, i = 1, \ldots, N, \\
&q_{N+i,j} = (1 - p_{N,j}) \prod_{k=1, k\neq i}^{j-1} p_{N,k}, i, j = 1, \ldots, N, i \neq j, \\
&q_{2N+i,i} = \prod_{k=1}^{i-1} p_{N,k}, i = 1, \ldots, N, \\
&q_{2N+i,j} = (1 - p_{N,j}) \prod_{k=1, k\neq i}^{j-1} q_{N,k}, i, j = 1, \ldots, N, i \neq j, \\
&q_{i,0} = p_N, i = 1, \ldots, N, \\
&q_{0,0} = 1, \\
&q_{i,j} = 0, \text{otherwise.}
\end{aligned} \quad (34)$$

TABLE II: The default system parameters

Notation	Description	Values
λ_A	THz BS density	0.001 units/m^2
λ_B	density of blockers	0.3 units/m^2
r_B	blocker radius	0.4 m
h_B	blocker height	1.7 m
h_U	UE height	1.5 m
h_A	THz BS height	4 m
v	blocker speed	1 m/s
P_T	BS emitted power	2 W
ζ_T	path loss exponent in non-blocked state	2.1
M_T	shadow fading margin	3 dBi
M_I	interference margin	3 dBi
K	absorption coefficient	0.2
δ	array switching time	2 μs
T_P	periodic beam update interval	10 ms
N_T	BS antenna array configurations	64x64
N_U	UE antenna array configurations	4x4
N	number of THz BSs	1-10
N_0	density of noise	-84 dBi
$\Delta\theta$	mean displacement around Ox	0.1°
$\Delta\phi$	mean displacement around Oy	0.1°

The time diagram of the communication pattern for periodic design scheme is shown in Fig. 7. Observe that it also includes beam misalignment that triggers beamsearching procedures independently from LoS blockage events. The transition probability matrix can be found using (34), while the performance metrics for this scheme can be found similarly to the on-demand scheme with micromobility derived in Subsection IV-C.

V. Numerical Analysis

In this section, we elaborate our numerical results. As the periodic design scheme has a free parameter – periodic beam update interval, T_P, we start by comparing on-demand and periodic schemes for different values of T_P. Then, we proceed to evaluate the effect of dynamic blockage and micromobility on two considered metrics, mean spectral efficiency and fraction of time in outage for different system parameters. Finally, we evaluate the impact of multiconnectivity on these metrics by explicitly assessing the gains of different number of simultaneously supported THz BSs.

As shown in [15], the effect of Cartesian displacements, Δx and Δy, is negligible compared to yaw and pitch mobility. Thus, in the rest of this section, we concentrate on the effect of the latter parameters and keep Δx and Δy constant at 3 cm/s.

The default system parameters are provided in Table II, while the antenna array parameters are given in Section III.

TABLE III: Antenna parameters

Array	Gain, dBi	HPBW,^{o}	Config.	Iterative search, ms	Exhaustive search, ms
BS					
256x256	41.59	0.39	65536	131.1	2097.15
128x128	35.58	0.79	16384	32.8	524.28
64x64	29.58	1.59	4096	8.22	131.07
32x32	23.58	3.18	1024	2.08	32.76
UE					
16x16	17.58	6.37	256	8.7	2097.15
8x8	11.57	12.25	64	8.32	524.28
4x4	5.57	25.5	16	8.22	131.07
2x2	0.43	51	4	8.2	32.76

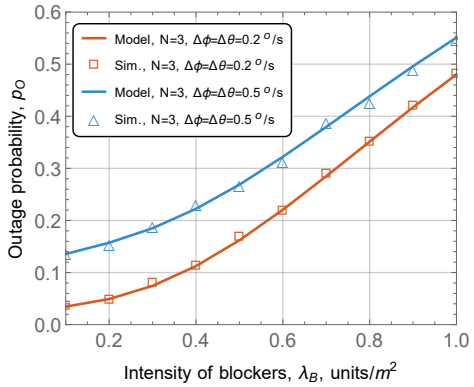

Fig. 8: Comparison of model and simulations results.

Since there are no cellular or WLANs systems operating in THz band yet, the chosen set of systems parameters attempts to provide the "best guess" of what first generation of THz communications systems might come with. Particularly, we selected the carrier frequency that is least affected by atmospheric absorption and utilized in the only THz standard available to date, IEEE 802.15.3d [55]. The emitted power is chosen as a trade-off between the typical power utilized in cellular systems and potential restrictions of THz electronics in first generation THz communications systems. In spite the future THz system may have slightly different system parameters we believe that the analysis below sheds some light on the qualitative trade-offs involved in the system design.

A. Accuracy Assessment

We start with assessing the accuracy of the developed model. To this aim, we have implemented the developed framework in our custom system level simulation (SLS) framework WinterSim utilized in the past for performance assessment of mmWave systems. The results of the comparison are provided in Fig. 8, where we illustrate outage probability for on-demand design scheme with micromobility as a function of blockers density for two values of yaw and pitch mobilities, $\Delta\phi = \Delta\theta = 0.2°$/s and $\Delta\phi = \Delta\theta = 0.5°$/s, and the degree of multi-connectivity $N = 3$. Here, as one may observe, the model results approximate simulation data well. Similar conclusions have been obtained for other system parameters and for this reason, in the rest of the numerical results section we solely rely upon the developed model.

B. Periodic Design Scheme

Consider first the periodic design scheme that is characterized by the free parameter – the time interval between regular beamsearching procedures, T_P. Recall, that according to the periodic design scheme the beamsearching procedure is initiated when either beam update interval expires or outage as a result of blockage or micromobility is experienced. To this aim, Fig. 9 and Fig. 10 shows outage probability and spectral efficiency for periodic and on-demand design schemes as a function of T_P, blockers density, λ_B, and coinciding yaw and pitch mobility, array switching time of $\delta = 2\mu$s, and the degree of multiconnectivity $N = 3$.

Analyzing the presented results, one may observe that for considered ranges of system parameters the periodic scheme performs worse in terms of both outage probability and spectral efficiency as compared to the on-demand scheme. We specifically recall that this scheme presumes that no additional external set of resources are dedicated for beamsearching procedure, i.e., the system needs to spend time for beamsearching it would otherwise utilize for information transmission. From this point of view, the provided results are logical and one may deduce that under $T_P \to \infty$ the periodic scheme reduces to on-demand one. Similar conclusions have been observed for other input parameters including other degrees of multiconnectivity.

As one may observe, for considered THz system configurations the periodic system design always leads to worse performance compared to on-demand design. Thus, we exclude this scheme from consideration in what follows.

C. Effect of System Parameters

We proceed with our numerical assessment campaign by observing the impact of blockage on the performance of the considered design schemes in Fig. 11. Particularly, it shows the outage probability and spectral efficiency as a function of blockers density for constant and coinciding yaw and pitch mobility of $\Delta\theta = \Delta\phi = 0.3$ deg/s, and two values of the degree of multiconnectivity, $N = 1$ and $N = 3$. As one may observe analyzing the presented results, for both $N = 1$ and $N = 3$ the

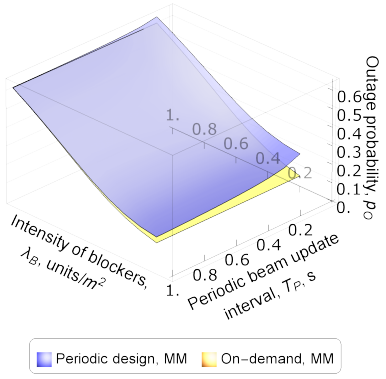

(a) Outage probability, $\Delta\phi = 0.1$ degrees/s

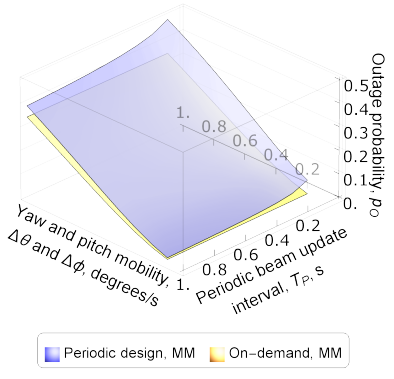

(b) Outage probability, $\lambda_B = 0.1$ units/m^2

Fig. 9: Outage probability: periodic and on-demand schemes.

best performance in terms of outage probability and spectral efficiency is observed for the ideal design scheme, where the beamsearching time is assumed to be zero. Furthermore, for $N = 1$ the on-demand scheme without micromobility performs only slightly worse than the ideal scheme. However, the performance of on-demand scheme in presence of micromobility drastically differs for $N = 1$ and for $N = 3$. First of all, one may notice that by increasing the degree of multiconnectivity from one to three the gap between the on-demand scheme without micromobility and the ideal scheme increases. The rationale is that the UE starts to spend more time being connected to farther BSs having worse spectral efficiency even when closer ones already return from the blocked state. Thus, the gain of utilizing multiconnectivity for mitigating blockage impairments decreases with the number of simultaneously supported links.

Observing the results of on-demand scheme with micromobility one may notice that its outage and spectral efficiency performance for $N = 1$ is drastically worse compared to the other two schemes. However, for the case of $N = 3$ both metrics significantly improve, especially, for small blockers densities, i.e., up to 0.5 bl./m^2. In this interval, this scheme stays close to the ideal scheme with $N = 3$ and even outperforms the ideal scheme and on-demand scheme without micromobility with $N = 1$. The latter is explained by the fact that micromobility forces UE to re-select BSs more frequently increasing the time spent on BSs having better spectral efficiency. Thus, we

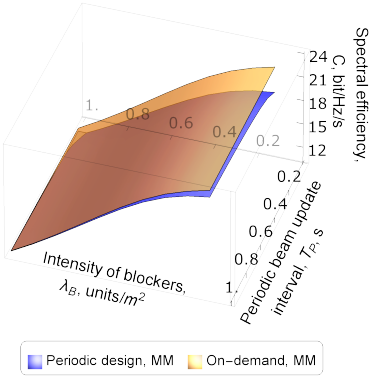

(a) Spectral efficiency, $\Delta\phi = 0.1$ degrees/s

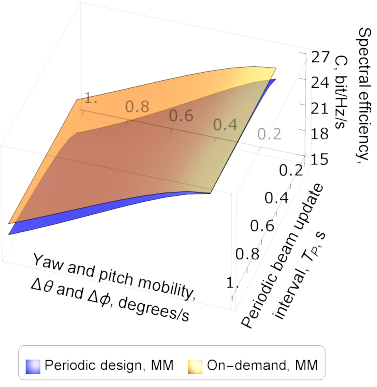

(b) Spectral efficiency, $\lambda_B = 0.1$ units/m^2

Fig. 10: Spectral efficiency: periodic and on-demand schemes.

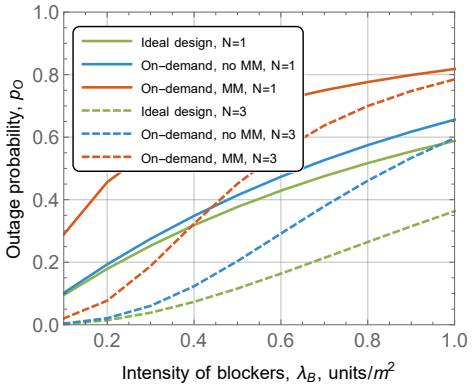

(a) Outage probability

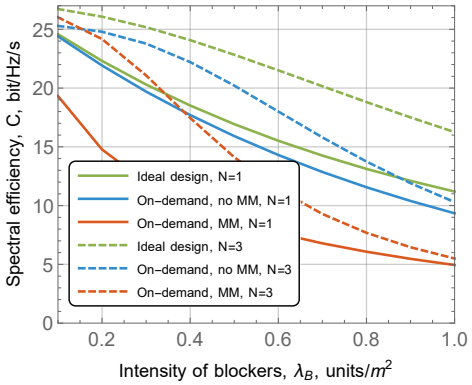

(b) Spectral efficiency

Fig. 11: Considered metrics as function of blocker intensity.

conclude that the positive effect of multiconnectivity increases in presence of UE micromobility.

Having revealed the effect of micromobility we now proceed to characterize its impact quantitatively. To this end, Fig. 12 shows the outage probability and spectral efficiency as a function of yaw and pitch mobility, $\Delta\theta$ and $\Delta\phi$, for considered design options, two degrees of multiconnectivity, $N = 1, 3$, and constant blockers density of $\lambda_B = 0.3$ units/m^2.

Analyzing the results presented in Fig. 12, we observe that the ideal and on-demand schemes without micromobility are characterized by constant outage probabilities and spectral efficiencies. The difference between them is attributed to the effect of blockage. On the other hand, the on-demand scheme with the micromobility effect is drastically affected by yaw and pitch movements. In prat ice, it implies that this scheme is heavily affected by the type of applications utilized by the user. Specifically, analyzing the case of $N = 3$ one may observe that depending on the yaw and pitch mobility velocity the system may change its operational regime from acceptable having outage probability of slightly less than 5% and spectral efficiency of around 25 bits/Hz/s to incredibly poor spending more than 40% of time in outage conditions and having much reduced spectral efficiency of around 15 bits/Hz/s.

Having characterized the effect of micromobility we now proceed considering the system response to different types of beamsearching procedure. Fig. 13 shows the outage probability and spectral efficiency as a function of yaw and pitch mobility, $\Delta\theta$ and $\Delta\phi$, for on-demand design options, degrees

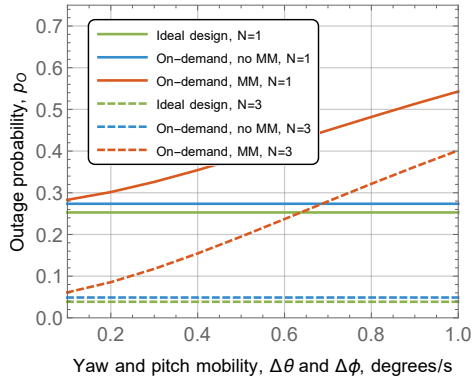

(a) Outage probability

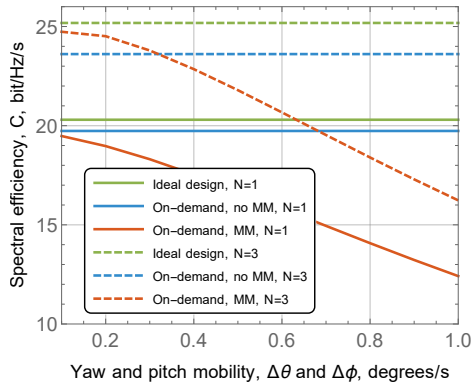

(b) Spectral efficiency

Fig. 12: Considered metrics as function of yaw/pitch mobility.

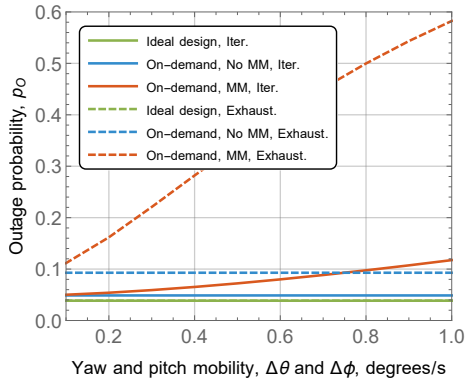

(a) Outage probability

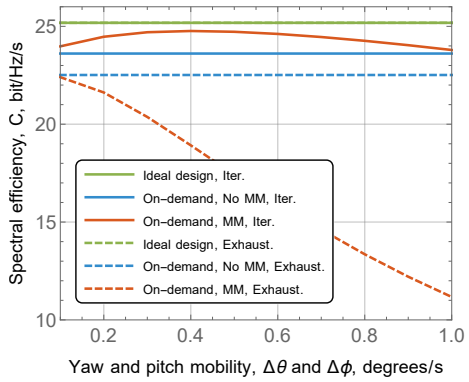

(b) Spectral efficiency

Fig. 13: Considered metrics as function of yaw/pitch mobility.

of multiconnectivity of $N = 3$, and constant blockers density $\lambda_B = 0.3$ bl./m^2. Recall, that the exhaustive and hierarchical are characterized by $T_B N_U N_T \delta$ and $T_B(N_U + N_T)\delta$ beamsearch time, where N_U and N_T are the number of UE and THz BS antenna array configurations and δ is the array switching time set to 2 μs. Note that the performance of the ideal scheme with hierarchical and exhaustive beamsearching coincides with each other as no beamsearching delays are taken into account. The constant gap between the ideal and on-demand scheme without micromobility reflects the performance degradation induced by the blockage. In its turn, the performance of the on-demand scheme with micromobility impairments heavily depends on the type of beamsearching procedure. For exhaustive search, the performance of this scheme is significantly worse compared to the other two schemes with the same search procedure. However, for smaller beamsearching time associated with the hierarchical algorithm, the outage probability of this scheme is comparable to the ideal scheme and on-demand scheme without micromobility impairments. Moreover, the spectral efficiency has a clear maximum attained for considered system parameters at $\Delta\phi = \Delta\theta \approx 0.5$ deg/s. At this point, the spectral efficiency approaches that of the ideal scheme. Thus, we may conclude that in future THz deployments the choice of the system parameters should account for the micromobility properties of the applications utilizing the wireless channel.

The usage of massive antenna arrays at BS is critical for THz communications to overcome severe path losses. To this end, in Fig. 14 and Fig. 15 we illustrate the outage and spectral efficiency as a function of the number of BS configurations, i.e., $N_T \times N_T$ and $N_U \times N_U$, respectively, fixed degree of multiconnectivity, $N = 3$, and constant blockers intensity $\lambda_B = 0.3$ units/m^2, yaw and pitch mobility of $\Delta\theta = \Delta\phi = 0.1$ deg/s. Analyzing the results presented in Fig. 14 and Fig. 15 one may observe, that the increase in the number of antenna elements at either BS or UE sides has a similar qualitative impact. For the ideal scheme and on-demand scheme without micromobility the response of the system is straightforward, i.e., the increase in the number of antenna elements results in a linear increase in spectral efficiency, while the outage probability remains constant. The on-demand scheme with micromobility impairments is characterized by more complex behavior. Particularly, for considered system parameters, there is a clear maximum attained for 128×128 and 4×4 BS and UE sides antenna configurations, respectively. Furthermore, the impact of UE antenna array is more profound. Thus, we may conclude that antenna arrays size is another parameter that can be varied adaptively to achieve the optimal spectral efficiency in prospective THz access systems deployments.

D. Effect of Multiconnectivity

Having studied the effects of system parameters on performance of the THz deployments for considered design options, we are now in the position to investigate the number of simultaneously supported THz BSs, i.e., the degree of multiconnectivity. To this end, Fig. 16 shows the effect of

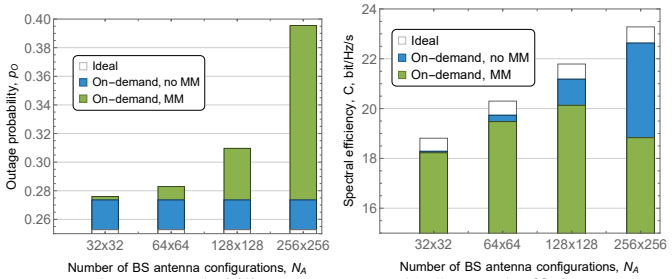

(a) Outage probability (b) Spectral efficiency

Fig. 14: Metrics as function of BS antenna elements.

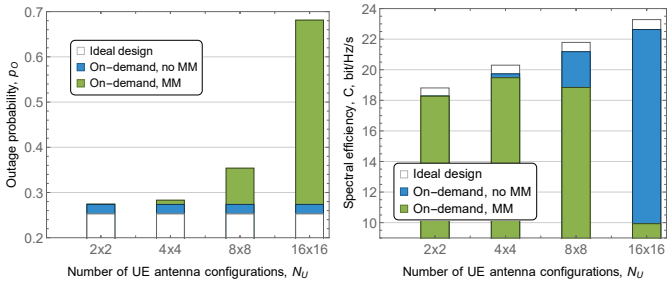

(a) Outage probability (b) Spectral efficiency

Fig. 15: Metrics as function of UE antenna elements.

degree of multiconnectivity on considered metrics for blockers intensity $\lambda_B = 0.3$, yaw and pitch mobility of 0.3 deg/s.

Analyzing the presented data one may conclude, that irrespective of the design scheme most of the gain comes from the nearest few THz BS for both outage probability and spectral efficiency. Particularly, for the on-demand scheme with the effect of micromobility the use of just three THz BS allows improving outage probability by 46 % and spectral efficiency by 21 %. Notice that the spectral efficiency gains achieved by other considered schemes for the same increase in the degree of multiconnectivity are smaller supporting our observation that micromobility impairments allow amplifying the multiconnectivity gains. Another critical observation is that in presence of micromobility high degrees of multiconnectivity (i.e., greater than three) also lead to higher gains with respect to the other two schemes even outperforming the on-demand scheme with only blockage impairments taken into account.

VI. Conclusion

The prospective THz cellular communications systems are expected to utilize massive antenna arrays at THz BS sides to compensate for extreme path losses. In addition to the dynamic blockage, these systems are expected to be affected by UE micromobility. In this paper, we developed a system-level mathematical framework for assessing the joint effect of micromobility and dynamic human body blockage on outage and spectral efficiency in future dense THz BS deployments. The framework is utilized to derive the metrics of interest for several typical system design schemes and different beam-searching algorithms with and without multiconnectivity.

Our results demonstrate that the impact of UE micromobility is not strictly negative and strongly depends on the system parameters. Particularly, the multiconnectivity functionality improves outages and spectral efficiency for small

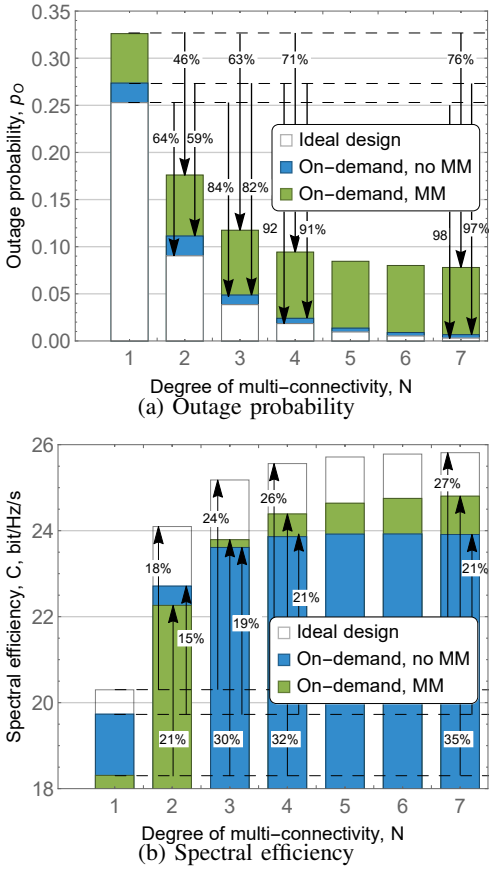

(a) Outage probability

(b) Spectral efficiency

Fig. 16: Metrics as function of degree of multiconnectivity.

and medium blockers density (up to 0.5 bl./m^2) under both blockage and micromobility impairments leading to spectral efficiency comparable to that of the ideal system with zero beamsearching times. There is also an optimal point for the on-demand beamsearching scheme, where spectral efficiency is maximized. In general, the gains of utilizing multiconnectivity for mitigating micromobility impairments increase with the number of simultaneously supported links and eventually lead to better performance compared to the system affected by blockage only. We also note that micromobility may happen much more frequently compared to the blockage events, as even small angular velocity at UE leads to the extreme linear velocity of the center of the beam. Given the current antenna array switching time, which is on the order of few microseconds, UE is forced to spend significant time in outage. As a result, for efficient utilization of THz resources, a significant improvement in the array switching time is needed. Thus, in future THz deployments, the choice of the system parameters should account for the micromobility properties of the applications utilizing the wireless channel.

Finally, we stress that although the absorption is an inherent phenomenon of THz band and may vary depending on the band of interest reducing the coverage of BSs, the qualitative results presented in the paper remain qualitatively intact for all values of K. This is critically important as the bands for both commercial 6G cellular systems and unlicensed Wi-Fi/WiGig-like solutions are not standardized yet. Thus, the qualitative results reported in our study are valid across the

whole considered range of THz frequencies.

REFERENCES

[1] S. Dang, O. Amin, B. Shihada, and M.-S. Alouini, "What should 6G be?," *Nature Electronics*, vol. 3, no. 1, pp. 20–29, 2020.

[2] P. Yang, Y. Xiao, M. Xiao, and S. Li, "6G wireless communications: Vision and potential techniques," *IEEE Network*, vol. 33, no. 4, pp. 70–75, 2019.

[3] T. S. Rappaport, Y. Xing, O. Kanhere, S. Ju, A. Madanayake, S. Mandal, A. Alkhateeb, and G. C. Trichopoulos, "Wireless communications and applications above 100 GHz: Opportunities and challenges for 6G and beyond," *IEEE Access*, vol. 7, pp. 78729–78757, 2019.

[4] M. Polese, J. Jornet, T. Melodia, and M. Zorzi, "Toward end-to-end, full-stack 6G terahertz networks," *IEEE Communications Magazine*, vol. 58, no. 11, pp. 48–54, 2020.

[5] J. M. Jornet and I. F. Akyildiz, "Channel modeling and capacity analysis for electromagnetic wireless nanonetworks in the terahertz band," *IEEE Transactions on Wireless Communications*, vol. 10, no. 10, pp. 3211–3221, 2011.

[6] G. A. Siles, J. M. Riera, and P. Garcia-del Pino, "Atmospheric attenuation in wireless communication systems at millimeter and thz frequencies [wireless corner]," *IEEE Antennas and Propagation Magazine*, vol. 57, no. 1, pp. 48–61, 2015.

[7] V. Petrov, M. Komarov, D. Moltchanov, J. M. Jornet, and Y. Koucheryavy, "Interference and sinr in millimeter wave and terahertz communication systems with blocking and directional antennas," *IEEE Transactions on Wireless Communications*, vol. 16, no. 3, pp. 1791–1808, 2017.

[8] B. A. Bilgin, H. Ramezani, and O. B. Akan, "Human blockage model for indoor terahertz band communication," in *2019 IEEE International Conference on Communications Workshops (ICC Workshops)*, pp. 1–6, IEEE, 2019.

[9] P. Boronin, V. Petrov, D. Moltchanov, Y. Koucheryavy, and J. M. Jornet, "Capacity and throughput analysis of nanoscale machine communication through transparency windows in the terahertz band," *Nano Communication Networks*, vol. 5, no. 3, pp. 72–82, 2014.

[10] J. M. Jornet and I. F. Akyildiz, "Femtosecond-long pulse-based modulation for terahertz band communication in nanonetworks," *IEEE Transactions on Communications*, vol. 62, no. 5, pp. 1742–1754, 2014.

[11] V. Petrov, D. Moltchanov, J. M. Jornet, and Y. Koucheryavy, "Exploiting multipath terahertz communications for physical layer security in beyond 5G networks," in *IEEE INFOCOM 2019-IEEE Conference on Computer Communications Workshops (INFOCOM WKSHPS)*, pp. 865–872, IEEE, 2019.

[12] R. Kovalchukov, D. Moltchanov, A. Samuylov, A. Ometov, S. Andreev, Y. Koucheryavy, and K. Samouylov, "Analyzing effects of directionality and random heights in drone-based mmwave communication," *IEEE Transactions on Vehicular Technology*, vol. 67, no. 10, pp. 10064–10069, 2018.

[13] A. Samuylov, D. Moltchanov, R. Kovalchukov, R. Pirmagomedov, Y. Gaidamaka, S. Andreev, Y. Koucheryavy, and K. Samouylov, "Characterizing resource allocation trade-offs in 5G NR serving multicast and unicast traffic," *IEEE Transactions on Wireless Communications*, vol. 19, no. 5, pp. 3421–3434, 2020.

[14] O. Chukhno, N. Chukhno, O. Galinina, Y. Gaidamaka, S. Andreev, and K. Samouylov, "Analysis of 3D deafness effects in highly directional mmWave communications," in *2019 IEEE Global Communications Conference (GLOBECOM)*, pp. 1–7, IEEE, 2019.

[15] V. Petrov, D. Moltchanov, Y. Koucheryavy, and J. M. Jornet, "Capacity and outage of terahertz communications with user micro-mobility and beam misalignment," *IEEE Transactions on Vehicular Technology*, vol. 69, no. 6, pp. 6822–6827, 2020.

[16] V. Petrov, D. Moltchanov, Y. Koucheryavy, and J. M. Jornet, "The effect of small-scale mobility on terahertz band communications," in *Proceedings of the 5th ACM International Conference on Nanoscale Computing and Communication*, pp. 1–2, 2018.

[17] 3GPP, "NR; Multi-connectivity; stage 2 (Release 16)," 3GPP TS 37.340 V16.0.0, December 2019.

[18] I. F. Akyildiz, J. M. Jornet, and C. Han, "Terahertz band: next frontier for wireless communications," *Physical Communication*, vol. 12, pp. 16–32, 2014.

[19] C. Han, X. Zhang, and X. Wang, "On medium access control schemes for wireless networks in the millimeter-wave and terahertz bands," *Nano Communication Networks*, vol. 19, pp. 67–80, 2019.

[20] I. F. Akyildiz, A. Kak, and S. Nie, "6G and beyond: The future of wireless communications systems," *IEEE Access*, vol. 3, pp. 133995–134030, 2020.

[21] M. Z. Chowdhury, M. Shahjalal, S. Ahmed, and Y. M. Jang, "6G wireless communication systems: Applications, requirements, technologies, challenges, and research directions," *IEEE Open Journal of the Communications Society*, vol. 1, pp. 957–978, 2020.

[22] K. Tekbıyık, A. R. Ekti, G. K. Kurt, and A. Görçin, "Terahertz band communication systems: Challenges, novelties and standardization efforts," *Physical Communication*, vol. 35, pp. 1–18, 2019.

[23] Y. Yuan, Y. Zhao, B. Zong, and S. Parolari, "Potential key technologies for 6g mobile communications," *Science China Information Sciences*, vol. 63, no. 4, pp. 1–19, 2020.

[24] J. Kokkoniemi, A. Boulogeorgos, M. Aminu, J. Lehtomäki, A. Alexiou, and M. Juntti, "Impact of beam misalignment on thz wireless systems," *Elsevier Nano Communication Networks*, vol. 24, pp. 1–9, 2020.

[25] R. Singh and D. Sicker, "Parameter modeling for small-scale mobility in indoor thz communication," in *2019 IEEE Global Communications Conference (GLOBECOM)*, pp. 1–7, IEEE, 2019.

[26] I. F. Akyildiz and J. M. Jornet, "Realizing ultra-massive mimo (1024× 1024) communication in the (0.06–10) terahertz band," *Nano Communication Networks*, vol. 8, pp. 46–54, 2016.

[27] C. Han, J. M. Jornet, and I. Akyildiz, "Ultra-massive mimo channel modeling for graphene-enabled terahertz-band communications," in *2018 IEEE 87th Vehicular Technology Conference (VTC Spring)*, pp. 1–5, IEEE, 2018.

[28] Z. Hossain, C. N. Mollica, J. Federici, and J. M. Jornet, "Stochastic interference modeling and experimental validation for pulse-based terahertz communication," *IEEE Transactions on Wireless Communications*, vol. 18, no. 3, pp. 4103–4115, 2019.

[29] V. Petrov, M. Komarov, D. Moltchanov, J. M. Jornet, and Y. Koucheryavy, "Interference analysis of ehf/thf communications systems with blocking and directional antennas," in *2016 IEEE Global Communications Conference (GLOBECOM)*, pp. 1–7, IEEE, 2016.

[30] C.-C. Wang, W.-L. Wang, and X.-W. Yao, "Interference and coverage modeling for indoor terahertz communications with beamforming antennas," *The Computer Journal*, vol. 63, no. 10, pp. 1597–1606, 2020.

[31] A. Shafie, N. Yang, Z. Sun, and S. Durrani, "Coverage analysis for 3D terahertz communication systems with blockage and directional antennas," in *2020 IEEE International Conference on Communications Workshops (ICC Worksops)*, pp. 1–7, IEEE, 2020.

[32] A. Shafie, N. Yang, and C. Han, "Multi-connectivity for indoor terahertz communication with self and dynamic blockage," in *ICC 2020-2020 IEEE International Conference on Communications (ICC)*, pp. 1–7, IEEE, 2020.

[33] J. Sayehvand and H. Tabassum, "Interference and coverage analysis in coexisting rf and dense terahertz wireless networks," *IEEE Wireless Communications Letters*, vol. 9, no. 10, pp. 1738–1742, 2020.

[34] A. Shafie, N. Yang, S. Durrani, X. Zhou, C. Han, and M. Juntti, "Coverage analysis for 3D terahertz communication systems," *IEEE Journal on Selected Areas in Communications*, vol. 39, no. 6, pp. 1817–1832, 2021.

[35] P. Nain, D. Towsley, B. Liu, and Z. Liu, "Properties of random direction models," in *IEEE 24th Annual Joint Conference of the IEEE Computer and Communications Societies*, vol. 3, pp. 1897–1907, March 2005.

[36] T. Kürner, A. Fricke, S. Rey, P. Le Bars, A. Mounir, and T. Kleine-Ostmann, "Measurements and modeling of basic propagation characteristics for intra-device communications at 60 GHz and 300 GHz," *Journal of Infrared, Millimeter, and Terahertz Waves*, vol. 36, no. 2, pp. 144–158, 2015.

[37] N. Khalid and O. B. Akan, "Wideband thz communication channel measurements for 5G indoor wireless networks," in *2016 IEEE International Conference on Communications (ICC)*, pp. 1–6, IEEE, 2016.

[38] V. Petrov, J. M. Eckhardt, D. Moltchanov, Y. Koucheryavy, and T. Kurner, "Measurements of reflection and penetration losses in low terahertz band vehicular communications," in *2020 14th European Conference on Antennas and Propagation (EuCAP)*, pp. 1–5, IEEE, 2020.

[39] L. S. Rothman *et al.*, "HITRAN: High-resolution transmission molecular absorption database," Harvard-Smithson Center for Astrophysics, www.cfa.harvard.edu, 2014.

[40] J. Kokkoniemi, J. Lehtomaki, and M. Juntti, "A discussion on molecular absorption noise in the terahertz band," *Elsevier Nano Communication Networks*, vol. 8, pp. 35–45, June 2016.

[41] J. Kokkoniemi, J. Lehtomäki, and M. Juntti, "Stochastic geometry analysis for mean interference power and outage probability in thz networks," *IEEE Transactions on Wireless Communications*, vol. 16, no. 5, pp. 3017–3028, 2017.

[42] R. Kovalchukov, D. Moltchanov, A. Samuylov, A. Ometov, S. Andreev, Y. Koucheryavy, and K. Samouylov, "Evaluating SIR in 3D millimeter-wave deployments: Direct modeling and feasible approximations," *IEEE Transactions on Wireless Communications*, vol. 18, no. 2, pp. 879–896, 2019.

[43] D. Moltchanov, P. Kustarev, and Y. Koucheryavy, "Analytical approximations for interference and sir densities in terahertz systems with atmospheric absorption, directional antennas and blocking," *Physical Communication*, vol. 26, pp. 21–30, 2018.

[44] V. Petrov, M. Komarov, D. Moltchanov, J. M. Jornet, and Y. Koucheryavy, "Interference and SINR in millimeter wave and terahertz communication systems with blocking and directional antennas," *IEEE Transactions on Wireless Communications*, vol. 16, pp. 1791–1808, March 2017.

[45] S. Singh, R. Mudumbai, and U. Madhow, "Interference analysis for highly directional 60-GHz mesh networks: The case for rethinking medium access control," *IEEE/ACM Transactions on Networking*, vol. 19, pp. 1513–1527, October 2011.

[46] A. B. Constantine *et al.*, "Antenna theory: analysis and design," *Microstrip Antennas, John Wiley & Sons*, 2005.

[47] M. Gerasimenko, D. Moltchanov, M. Gapeyenko, S. Andreev, and Y. Koucheryavy, "Capacity of multiconnectivity mmWave systems with dynamic blockage and directional antennas," *IEEE Transactions on Vehicular Technology*, vol. 68, no. 4, pp. 3534–3549, 2019.

[48] IEEE, "Telecommunications and information exchange between systems local and metropolitan area networks – specific requirements. Part 11. Amendment 3," IEEE standard for information technology, 2012.

[49] M. Gapeyenko, V. Petrov, D. Moltchanov, M. R. Akdeniz, S. Andreev, N. Himayat, and Y. Koucheryavy, "On the degree of multi-connectivity in 5g millimeter-wave cellular urban deployments," *IEEE Transactions on Vehicular Technology*, vol. 68, no. 2, pp. 1973–1978, 2019.

[50] D. Moltchanov, "Distance distributions in random networks," *Elsevier Ad Hoc Networks*, vol. 10, pp. 1146–1166, August 2012.

[51] V. Begishev, D. Moltchanov, E. Sopin, A. Samuylov, S. Andreev, Y. Koucheryavy, and K. Samouylov, "Quantifying the impact of guard capacity on session continuity in 3GPP New Radio systems," *IEEE Transactions on Vehicular Technology*, vol. 68, no. 12, pp. 12345–12359, 2019.

[52] M. Gapeyenko, A. Samuylov, M. Gerasimenko, D. Moltchanov, S. Singh, M. R. Akdeniz, E. Aryafar, N. Himayat, S. Andreev, and Y. Koucheryavy, "On the temporal effects of mobile blockers in urban millimeter-wave cellular scenarios," *IEEE Transactions on Vehicular Technology*, available online, 2017.

[53] M. Gapeyenko, A. Samuylov, M. Gerasimenko, D. Moltchanov, S. Singh, E. Aryafar, S.-p. Yeh, N. Himayat, S. Andreev, and Y. Koucheryavy, "Analysis of human-body blockage in urban millimeter-wave cellular communications," in *Communications (ICC), 2016 IEEE International Conference on*, pp. 1–7, IEEE, 2016.

[54] J. G. Kemeny, J. L. Snell, *et al.*, *Finite markov chains*, vol. 356. van Nostrand Princeton, NJ, 1960.

[55] V. Petrov, T. Kurner, and I. Hosako, "Ieee 802.15. 3d: First standardization efforts for sub-terahertz band communications toward 6g," *IEEE Communications Magazine*, vol. 58, no. 11, pp. 28–33, 2020.